Research Article **Open Access**

A. Mishra, J. Rocherullé, and J. Massera*

Ag-doped phosphate bioactive glasses: thermal, structural and *in-vitro* dissolution properties

DOI 10.1515/bglass-2016-0005
Received Feb 01, 2016; revised May 14, 2016; accepted Jun 04, 2016

Abstract: Ag doped-bioactive phosphate glasses were processed by traditional melt quenching technique with the concentration of Ag_2O ranging from 0 to 5 mol%. The Ag doping led to the depolymerization of the phosphate network which is accompanied by a decrease in the glass transition temperature. The processing window represented by ΔT ($\Delta T=T_x-T_g$) exhibited a maximum for glasses containing 2-3 mol% of Ag_2O. An increase in Ag content induced an increase in the glass dissolution rate. The precipitation of a Sr-CaP layer at the surface of the glass particulates was found to occur at shorter immersion time for the Ag containing glasses. The congruent dissolution and wide processing window of these Ag containing glasses may be of great interest for scaffold manufacturing from sintering of glass powders with antimicrobial properties.

1 Introduction

Since the discovery of the bioactive glass 45S5 (Bioglass®) by L.L. Hench [1] and S53P4 by Andersson *et al.* [2], much work has focused on tailoring the silicate bioactive glass composition to enable fiber drawing or powder sintering [3–5]. Studies show that typical silicate bioactive glasses have a crystallization kinetics that not only inhibits shaping at medium to high temperature but also reduce the glass's bioactivity [3, 6].

A. Mishra: Department of Electronics and Communications Engineering, Tampere University of Technology, Korkeakoulunkatu 3, FI-33720, Tampere, Finland
J. Rocherullé: Equipe Verres et Céramiques, UMR-CNRS 6226, Sciences Chimiques de Rennes, Université de Rennes I, F-35042 Rennes Cedex, France
***Corresponding Author: J. Massera:** Department of Electronics and Communications Engineering, Tampere University of Technology, Korkeakoulunkatu 3, FI-33720, Tampere, Finland; BioMediTech, University of Tampere and Tampere University of Technology, Biokatu 10/FI-33520 Tampere, Finland; Email: jonathan.massera@tut.fi

Phosphate bioactive glasses (PBGs) arise as a potential substitute to the typical silicate glasses. The chemical resistance of phosphate glasses can be tailored to suit different applications. The time required for complete degradation can be adjusted from hours to years [7]. PBG demonstrate bioactivity and are promising materials for use in bone repair and reconstruction [8]. Furthermore PBG are known to possess thermal properties showing wider processing window as evidenced by the large number of bioactive phosphate fibers studied in the past years [9, 10].

Glasses within the $50P_2O_5$-$10Na_2O$-(40-x)CaO-xSrO composition exhibited a minimum in the dissolution when half of the CaO was replaced with SrO [11]. It was found that the dissolution rate is dependent on the glass structure and a reduction in the phosphate chain length leads to an increase in the chemical resistance. Furthermore, the proliferation and growth of gingival fibroblasts cells increased with increasing the SrO content. Whereas the SrO-free glass led to cell death within 24h, the CaO-free glass showed a cell count similar to the one measured at the surface of the glass S53P4 used as reference [12]. This is partially attributed to the decrease in initial dissolution rate when SrO is introduced in place of CaO in the glass. The effect of strontium ions both in the media and in the reactive layer also play an important role as discussed in [12]. However, despite those promising results, these metaphosphate glasses present a rapid initial dissolution rate and late precipitation of a reactive layer disabling the cells to efficiently attach for the first 1-3 days of culture [12]. This is in agreement with Salih *et al.* who showed that fast dissolving glasses did not allow for proper cell proliferation [13].

Metal ions such as Silver (Ag), Copper (Cu) or Cobalt (Co) just to cite a few can be added to glasses in order to give them unique properties or modify the existing physical or chemical properties for clinical applications. These ions are known to exhibit antimicrobial properties for example [14–16]. Ag is a popular choice as a dopant for several biomedical devices owing to its low toxicity to human cells and effectiveness against many types of microbial growth, even at low concentrations [17]. Ag ions in the form of nitrate, oxide are commonly found in several healthcare

Table 1: Glasses nominal compositions.

Glass	P_2O_5 (mol%)	CaO (mol%)	SrO (mol%)	Na_2O (mol%)	Ag_2O (mol%)
x=0	50	20	20	10	0
x=1	49.5	19.8	19.8	9.9	1
x=2	49	19.6	19.6	9.8	2
x=3	48.5	19.4	19.4	9.7	3
x=5	47.5	19	19	9.5	5

products, for *e.g.*, Ag coated catheters, wound dressing for example [17]. Ag based ointments have long been used to treat wounds susceptible to bacterial infections [18]. When PBGs are doped with Ag, the metal atoms are assumed to be incorporated in the structure [19]. As opposed to silicate glasses, PBG are known to have, in general, a congruent dissolution. Thus the rate of release of Ag ions, which depends upon the dissolution of the glass itself, can then be controlled if the Ag ions are added in PBG. Ahmed *et al.* developed silver-doped phosphate bioactive glasses with substitution of Na_2O for Ag_2O up to 15 mol%. Maximum antimicrobial effect was found to occur in glasses with 1 to 5 mol% of Ag_2O [14]. The structure and properties of the silver-doped glasses were also studied by the authors [20]. More recently, the investigation of silver-doped phosphate glasses with antimicrobial properties were also investigated for glasses with 65 and 70 mol% of P_2O_5 [21]. In this study an increase in the antimicrobial effect was seen with increasing the Ag content while similar effect was found on Ag-free glasses when increasing the phosphate content. However, in these studies, the phosphate content was 50 mol% or greater. The fast dissolution rate of glass in the P_2O_5-CaO-Na_2O family, with P_2O_5 content greater that 50 mol%, was found to inhibit growth and bone antigen expression. On the other hand the glasses with slow solubility upregulated the proliferation of cells [13]. Based on the previous research on Sr-containing bioactive glasses it appears that despite a P_2O_5 content of 50% gingival fibroblast cells can attach and proliferate [12]. Thus it is of tremendous interest to study the impact of Ag doping on this glass composition and assess whether antimicrobial Ag-doped strontium containing phosphate glasses can be obtained.

In this paper we report on the effect of Ag doping on the thermal, structural and *in-vitro* dissolution properties of the phosphate bioactive glass previously studied in [12]. Ag_2O was introduced relative to the entire base glass as opposed to the typical isomorphic substitution. The reason for such doping was to maintain the same (Ca+Sr)/P ratio in the glass while lowering the phosphate content. The thermal properties as a function of Ag content were measured using a differential thermal analyzer (DTA). The structure was assessed by Fourier transformed infrared spectroscopy in attenuated total reflectance mode (FTIR-ATR). The dissolution test was performed in TRIS buffer solution in order to confirm the congruent dissolution of investigated glasses. The formation of a CaP layer at the surface of the glasses upon immersion in TRIS was evidenced by SEM/EDS and FTIR-ATR. Finally the ions released in solution were quantified using ion chromatography and ICP.

2 Materials and Methods

Glass preparation

Glasses with nominal composition $[(Ag_2O)_x\text{-}(0.5P_2O_5 \cdot 0.2CaO{\cdot}0.2SrO{\cdot}0.1Na_2O)_{100-x}]$ where x = 0, 1, 2, 3 and 5 mol% were prepared. The nominal compositions are reported in Table 1. The glasses were obtained by melting in a silica crucible in air. Analytical grade $CaCO_3$, $SrCO_3$, $NH_4H_2PO_4$, Ag_2O, $NaPO_3$ and Na_2SO_4 were used to prepare the batch. $Ca(PO_3)_2$ and $Sr(PO_3)_2$ were first prepared by heating $NH_4H_2PO_4$ and carbonates at 300°C during 2 hours to remove NH_3, H_2O and CO_2 then maintained 10 hours at 850°C and 750°C for the calcium and strontium samples, respectively. The batch was placed in a silica crucible and heated up to 1000 °C for 30 minutes. 1 wt% Na_2SO_4 was added to the batch to avoid the reduction of silver oxide into metallic silver. The melt was poured into a preheated brass mould and annealed at T_g+15°C for 30 minutes, then cooled down to Tg-50°C at 1 °C·min^{-1} and annealed during one hour to lower the internal stress. Finally, the furnace was turned off and the glass cooled to room temperature before removal. After melting, the glasses were analyzed with EDS and the composition was found to be in agreement with the nominal one, within the accuracy of the measurement (1.5 wt%). Despite the melting in silica crucible and the addition of Na_2SO_4, no Si or S were found in the analysis.

Physical properties

The density of the glasses was measured using Archimedes principle with an accuracy of ±0.02 g/cm^3. Ethanol was used as immersion liquid and the measurement was performed on a polished glass bulk. Molar volume of the glasses was calculated using their density and molecular weight. Young's modulus (E) was measured by the ultrasonic velocity technique. This technique is based on time-of-flight measurements using the pulse-echo technique [22] with ±2 GPa as the accuracy value. Vickers microhardness (Hv) was measured by the indentation technique using a Matsuzawa® Digital Microhardness Tester MXT 70 with a pyramid shaped diamond indenter. A load of 0.4905 N was applied for 5 s for all the measurements which were performed at room temperature on polished surfaces. The displacement rate was the same on loading and unloading. All the characteristics were averaged over measurements on 10 indentations per sample. The accuracy is considered as better than ±0.2 GPa.

Thermal properties

Differential Thermal Analysis (DTA, Netzch JUPITER F1) of all the glasses was carried out at a heating rate of 10 °C/min, in a Pt crucible and with a flow of 50 ml/min of N_2. The T_g (glass transition temperature), T_x (crystallization temperature) and T_p (crystallization temperature) were assessed from the obtained thermogram. T_g was determined as the inflection point of the endotherm obtained by taking first derivative of the DTA curve with an accuracy of 2 °C. The T_x was taken as the onset of the crystallization peak and T_p as the maxima of the exotherm. All measurements were obtained with an accuracy better than ±3°C

Structural Properties

The IR absorption spectra for all glass powders before and after immersion in TRIS were recorded with Perkin Elmer Spectrum One FTIR Spectrophotometer in Attenuated Total Reflectance (ATR) mode. All spectra were recorded in the range 600–1600 cm^{-1}, corrected for Fresnel losses and were normalized to the band with maximum intensity. Each spectrum is an average of 8 scans and has a resolution of 1 cm^{-1}.

Optical Properties

The UV-Vis absorption spectra for all the glasses were recorded in the range 200–1600 nm at room temperature using a UV-3600 Plus UV-VIS-NIR Spectrophotometer Shimadzu. The glass samples used for this measurement were 2 mm thick and optically polished.

In-vitro dissolution

The glasses were crushed and sieved to obtain powder with size ranging from 125 to 200 µm. These particles were immersed in TRIS buffer solution and placed in an incubating shaker HT Infors Multitron at 37°C, 100 rpm to obtain laminar flow mixing without moving the particles. The mass to volume ratio was kept constant at 75 mg of glass for 50 ml TRIS. Immersion test was conducted for up to 4 weeks. The pH of the solution was measured before and after immersion using pH ion analyzer Mettler Toledo SevenMultimeter with accuracy better than ±0.02. The pH of the solutions containing glass was compared to a TRIS blank sample. The pH of the blank solution was found to remain unchanged throughout the testing period. Post immersion, the glass powder was recovered, washed with acetone and dried for FTIR-ATR and SEM-EDS analysis. 10 ml of the TRIS solution containing glassy powder was diluted in 90ml of ultra-pure water for ICP-OES measurement Inductively coupled plasma - Optical emission spectrometer (ICP-OES; Optima 5300DV, Perkin Elmer) was employed to quantify the amount of P, Sr, Ca and Na ions found in the TRIS solution after glass immersion. The value obtained for each ions was compared to the value obtained for the blank samples (only TRIS). The TRIS samples used as blanks were analyzed to ensure that the concentration of P, Ca, Sr and Na was consistently 0, or under the detection limit, as no such ions should be present in TRIS buffer solutions.

Imaging and elementary analysis

Scanning electron microscopy (SEM), using a JEOL JSM 7100F apparatus, was used for high-resolution imaging of the sample surfaces (Pressure: 10^{-4} Pa, accelerator voltage: 20 kV). Energy Dispersive X-Ray Spectroscopy (EDS) was used as the chemical microanalysis technique used in conjunction with SEM. The associated detector (EDS SDD X-Max 80mm2 Oxford Instruments AZtecEnergy) allows one to identify what particular elements are and their relative atomic proportions. This powerful tool of the elemen-

Table 2: Thermal and mechanical properties.

Glass	T_g(±3°C)	T_x(±3°C)	T_p(±3°C)	$\Delta T=T_x-T_g$ (±6°C)	HV (±0.2GPa)	E (±2GPa)
x = 0	436	550	603	114	2.3	55
x = 1	430	554	583	124	2.2	56
x = 2	428	567	611	139	2.2	55
x = 3	420	560	597	140	2.2	55
x = 5	418	546	587	128	2.2	56

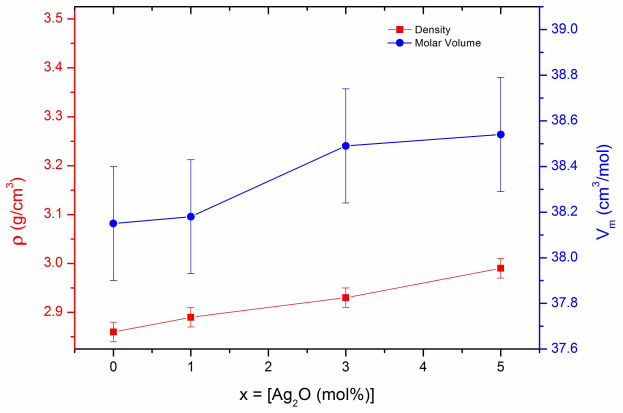

Figure 1: Density (ρ) and molar volume (V_m) of the investigated glasses.

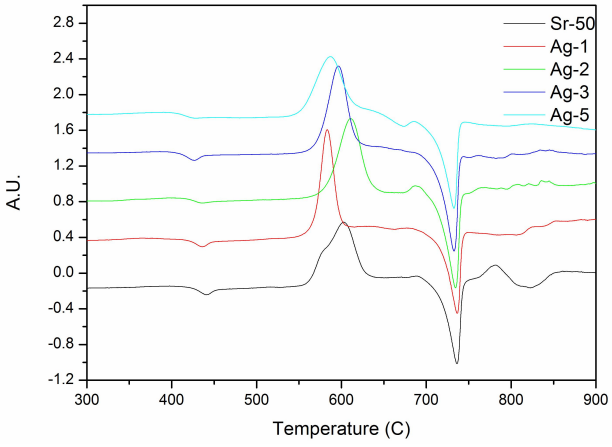

Figure 2: DTA thermogram of the investigated glasses.

tal analysis can identify elements heavier than Be with a spatial resolution better than 1 μm^3, corresponding to a smallest spot size of about 1 μm^2, and the accuracy is ±1% for polished bulk target in this case where pure standards are collected on site.

3 Results

The glasses of investigation with composition $[(Ag_2O)_x$-$(0.5P_2O_5 \cdot 0.2CaO{\cdot}0.2SrO{\cdot}0.1Na_2O)_{100-x}]$ where x = 0, 1, 2, 3 and 5 mol% were analyzed using EDS/SEM. All the compositions were found to be in agreement with the nominal one within the accuracy of the measurement. As already mentioned in the previous section, we assume that no Si was found despite using a silica crucible. Nevertheless, the Sr $L_{\alpha 1}$ EDX peak located at 1806 keV can mask the Si K peak at 1740 keV, however the low melting temperature (1000°C) and the short fining time used for the glass synthesis, allows to prevent the silica dissolution in phosphate melts, as stated in previous studies conducted on phosphate glasses which do not contain Sr and for which, the chemical compositions were checked by EDS [23, 24].

Figure 1 presents the density (ρ) and molar volume (V_m) of the investigated glass as a function of Ag_2O content. With an increase in Ag_2O, the density increases while the molar volume remains constant, within the accuracy of the measurements.

The thermal properties of the investigated glasses are reported in Table 2 and the DTA traces are shown in Figure 2. With an increase in Ag_2O, the glass transition temperature T_g decreases whereas T_x and T_p exhibit a maximum for the glass with x = 2 mol%. ΔT ($\Delta T=T_x-T_g$), which is a gauge of glass's resistance to crystallization, is also found to present a maximum for glasses with x = 2 and 3 mol%. It is interesting to note that the glass with x = 1 mol% possesses a sharper crystallization peak as compared to the other glasses under investigation. In addition, the Young's modulus and the Vickers microhardness were determined for all the glass samples. These values, summarized in Table 2, which do not exhibit any difference, when considering the accuracy of the measurements, are 55 GPa and 2.2 GPa for the Young's modulus and for the Vickers microhardness, respectively. The glass's structural properties were assessed using FTIR-ATR and Raman spectroscopy. The IR spectra of the glasses are shown in Figure 3a. All spectra were normalized to the band located

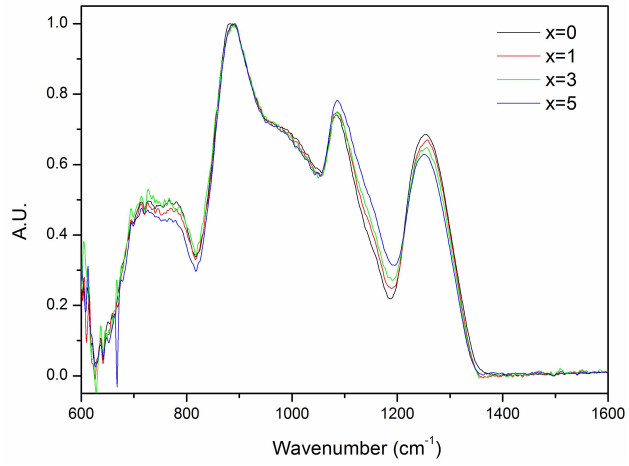

(a)

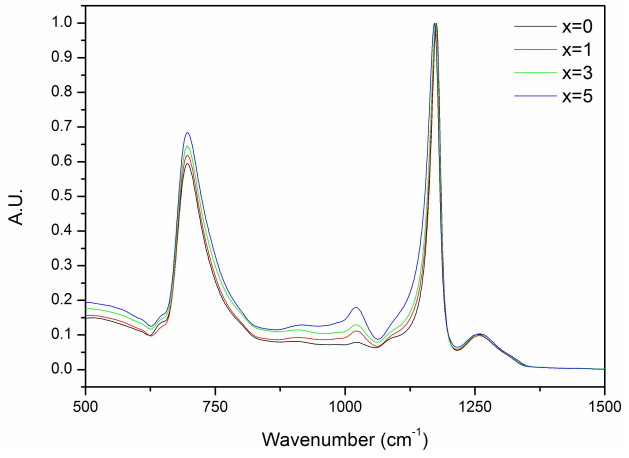

(b)

Figure 3: FTIR-ATR a) and Raman b) spectra of the investigated glasses.

at ~880 cm^{-1}. The spectra exhibit five absorption bands located around 1260, 1085, 880, 775 and 718 cm^{-1} and two shoulders at ~1154 and 980 cm^{-1}. With an increase in Ag_2O, all bands remained unchanged in terms of intensity and shape, except for the band at 1260 cm^{-1} which decreases in intensity.

Figure 3b presents the Raman spectra of the glasses. All spectra were normalized to the band with maximum intensity peaking at ~1175 cm^{-1}. The spectra exhibit four bands and one shoulder which are all characteristics of the metaphosphate network. With an increase in Ag_2O, all bands are found to shift to lower wavenumber. The bands at 695 and 1020 cm^{-1} as well as the shoulder at 1090 cm^{-1} are all found to increase in intensity as compared to the band at 1175 cm^{-1}.

Glass powder of each composition was immersed in TRIS solution for up to 672 hours. After 0, 24, 72, 168, 336 and 672h of immersion, the particles were rinsed and dried for analyses using FTIR-ATR and EDS/SEM. The solution was diluted ten times for ion concentration analysis using ICP-OES.

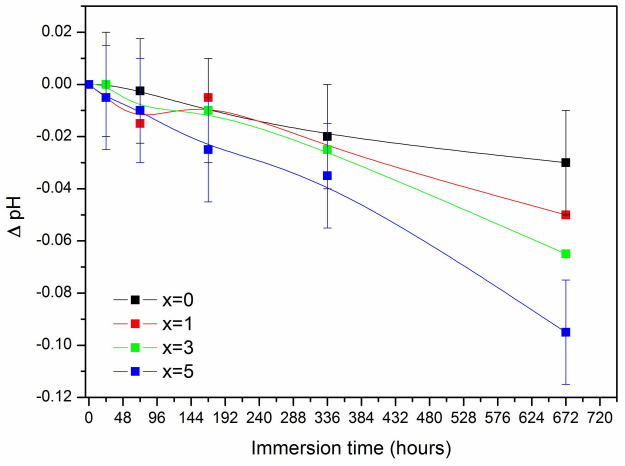

Figure 4: Change in pH as a function of immersion time.

At each immersion time, the pH of the solution was measured and the change in pH (as compared to the pH of the blank TRIS solution) is presented in Figure 4. As the immersion time increases, the pH of the solutions containing the newly prepared glasses decreased. One can notice that an increase in Ag_2O leads to a stronger decrease in the solution pH.

The ion concentration in solution was quantified using ICP-OES. The evolution over time of the Ca, Sr, Na, and P concentrations is presented in Figure 5a, b, c and d, respectively. With an increase of the immersion time, an increase in the Ca, Sr, Na and P concentration is seen. The release of ions is greater with an increase in Ag_2O. This increase is seen despite the decrease in these ions in the base glass (Table 1), due to the Ag doping.

The FTIR-ATR spectra of the glasses with silver content x = 0 a), x = 1 b), x = 3 c) x = 5 d) as a function of immersion time are presented in Figure 6. For immersion up to 72 h, no significant changes could be seen in the FTIR-ATR spectra of all investigated glasses. With an increase in immersion time, all glasses exhibit a decrease in intensity and shift to lower wavenumber of the bands located at 1260 and 775 cm^{-1}. The main band, at 890 cm^{-1}, is also found to shift to lower wavenumber. The band at 1085 cm^{-1}, is found to decrease in the glass with x = 0, whereas, for all Ag-containing samples the band decrease in intensity for immersion up to 336 h and then increases in intensity and shift to higher wavenumber for longer immersion time. All spectra for the Ag-containing glasses exhibit the appearance of new bands at 988 and 1030 cm^{-1}.

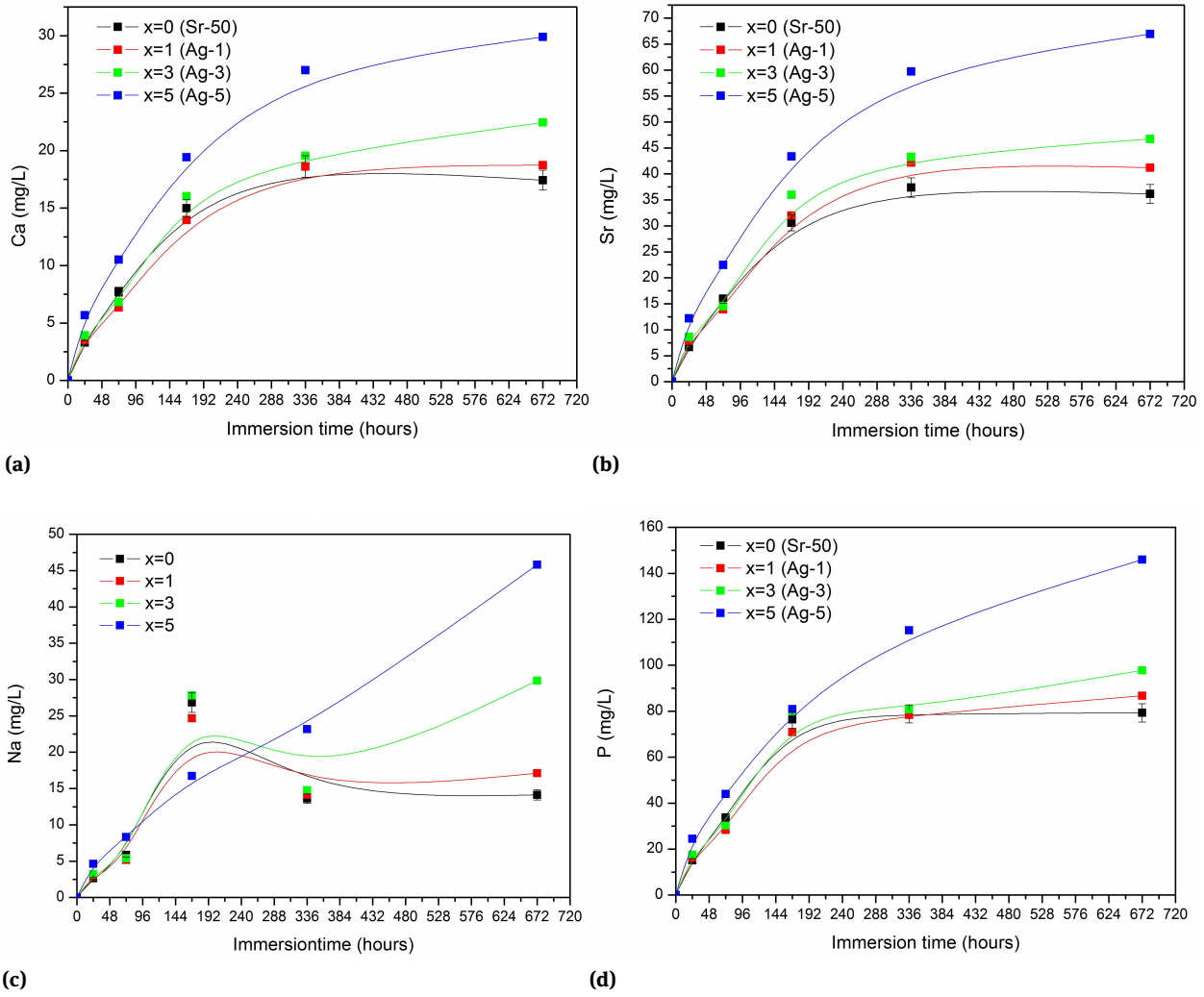

Figure 5: Ca a), Sr b), Na c) and P d) concentration in TRIS solution as a function of immersion time.

Comparison of the spectra for all glasses when immersed for 672 h is presented in Figure 6e. It is clearly seen that the rise of the peak at 1150 and the intensity of the new bands at 988 and 1030 cm^{-1} are higher with increasing Ag_2O.

The SEM images of the glasses with x = 0 after 672 h of immersion and of the glasses with x = 3 and 5 mol% after 336 h of immersion are presented in Figure 7a, 7b and 7c, respectively. At 168 h, no change in the glass surface composition could be evidenced by EDS analysis. After 672 h of immersion, no layer could be seen (or only sparsely) at the surface of the glass with x = 0, while a reactive layer could be seen at the surface of the Ag-containing glasses already after 336h of immersion. We noticed that its thickness grew thicker with increasing the immersion time. From SEM images the layer grew up to 5 µm for the glass with 5 mol% Ag_2O. EDS analysis revealed that this layer was rich in Ca and P and contained a significant amount of Sr. It appear clear that the layer thickness increases with increasing Ag_2O, whereas the layer composition was identical at the surface of all materials

4 Discussion

The aim of this research is to better understand the impact of Ag doping on the thermal, structural and dissolution of a phosphate bioactive glass.

Doping the glass Sr-50, which was found in the past to be a promising bioactive glass [11, 12], with Ag led to an increase in the density. This was expected as Ag has a larger mass than all the other elements present in the glass composition. However, the addition of Ag does not significantly change the molar volume indicating that the Ag acts

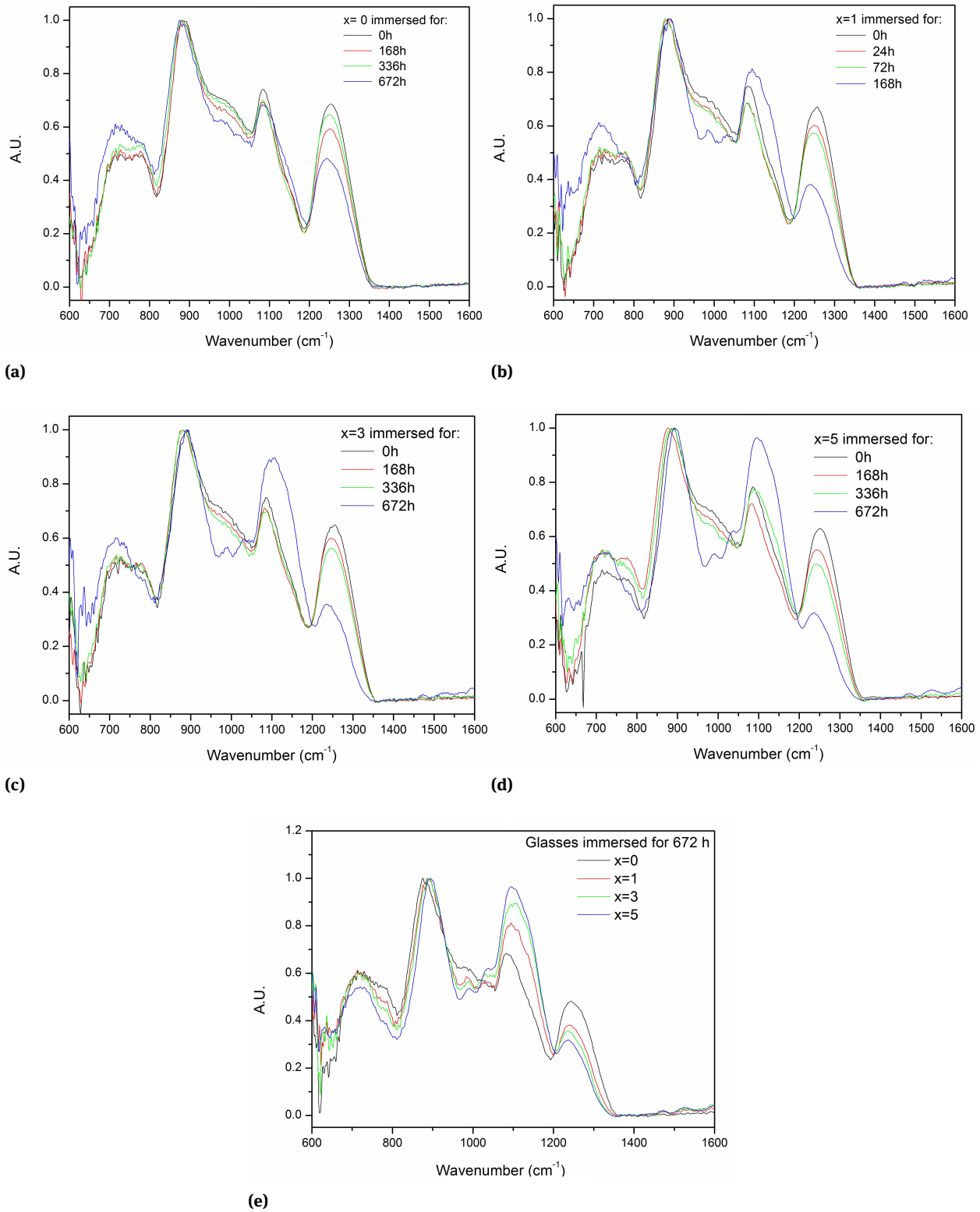

Figure 6: FTIR-ATR of the glass x = 0 a), x = 1 b), x = 3 c) and x = 5 d) as a function of immersion time and all glasses immersed for 672 h in TRIS e)

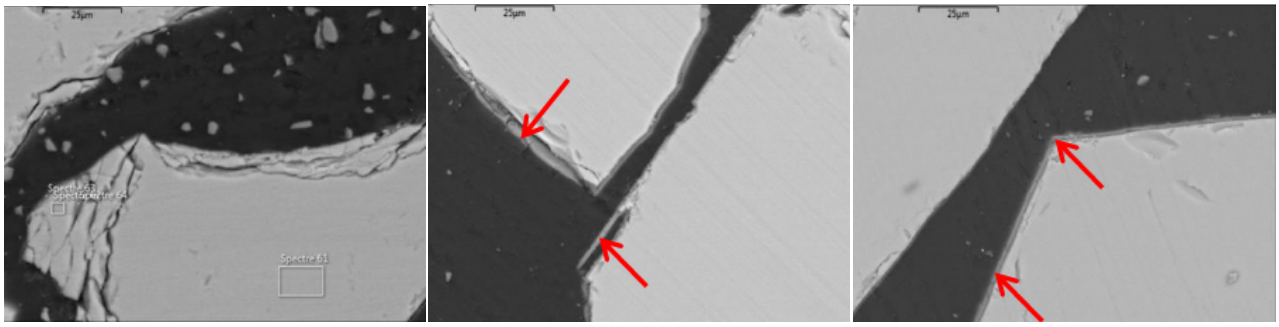

(a) (b) (c)

Figure 7: SEM images of the glasses with x = 0 after 672 h of immersion a) and of the glasses with x = 3 b) and 5 c) after 336 h of immersion.

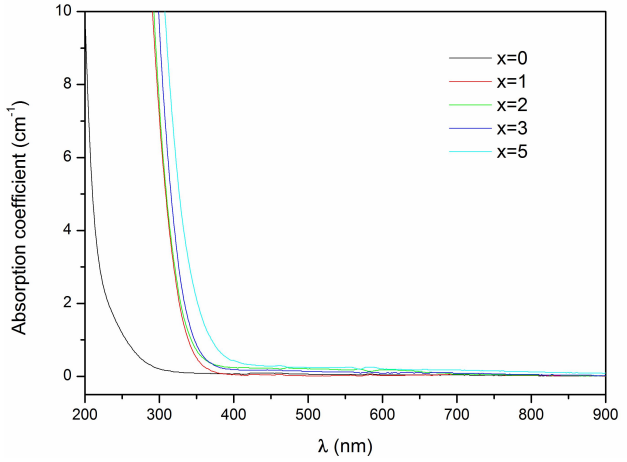

Figure 8: UV-Vis absorption spectra of the glasses of investigation.

as a monovalent cation in the phosphate vitreous network with a similar ionic radius and similar positions than the other modifiers in the network. However the redox activity of a glass melt is definitely a function of the composition and, at first sight, it is generally found that increasing basicity favors the upper oxidation state for most redox couples [25]. Compared to silicon oxide, phosphorus pentoxide is characterized by a lower value of the optical basicity, 0.45 and 0.33, respectively [26]. As a result, phosphate glasses favor the lowest stable oxidation state, *i.e.* Ag^0. To avoid the presence of metallic silver droplets, the use of sodium sulfate as an oxidizing agent was necessary. The dissolution of the sulfate in the melt leads to the oxidation of the metallic silver according to the following chemical reactions:

$$SO_4^{2-} \rightleftharpoons O^{2-} + SO_2 + \frac{1}{2}O_2$$

$$2Ag + \frac{1}{2}O_2 \rightleftharpoons 2Ag^+ + O^{2-}$$

It results the chemical balance:

$$2Ag^0 + SO_4^{2-} \rightleftharpoons 2O^{2-} + 2Ag^+ + SO_2$$

Furthermore, to confirm that the use of Na_2SO_4 prevents formation of Ag nanoparticles, the UV-Vis spectra of the glasses were recorded and are presented in Figure 8. The absence of absorption band in the visible which could be a characteristic of the presence of Ag nanoparticles confirms that all the Ag is present as positively charged ions in the glasses under investigation. This is of particular interest since Ag^+ ions have been found to possess antimicrobial properties [19, 27].

The thermal properties of these glasses were recorded. With an increase in Ag_2O, the T_g decreases whereas T_x, T_p and ΔT show a maximum for the glasses with 2 and 3 mol% of Ag_2O. More interestingly the crystallization peak of the glass containing 1 mol% of Ag_2O was narrower than that of the other glasses (Fig. 2). This can be attributed to the change in crystallization mechanism of the glass induced by the occurring of a small amount of silver particle during the reheating of the glass. It is well known that Ag can be used in glass as nucleating agent [28]. It is also rather common to see Ag^0 formation upon heat treatment in glassy thin films or bulk [29, 30]. The decrease in T_g when Ag_2O increases may be explained by the lower cationic field strength value (Z/r^2) of silver (0.6) when compared to the others modifiers cations, namely sodium (1.06), strontium (1.56) and calcium (2.04), the coordination number being considered as 6 for the calculation.

Contrary to the glass transition temperature which is strongly dependent of the cationic strength, it has been demonstrated that the mechanical properties clearly depend on physical quantities related to the compactness or the energy of cohesion of the vitreous network, such as those defined in [31]. The steadiness of the molar volume, whatever the silver oxide content, leads to the same compactness and of the microhardness values. Regarding the

Table 3: FTIR-ATR and Raman bands attribution.

Wavenumber (cm^{-1})	Attribution	Reference
FTIR-ATR		
718–775	ν_s P-O-P in metaphosphate	[38]
880	ν_{as} P-O-P in Q^2	[33, 34]
980	ν_s PO_3^{2-} in Q^1	[34–36]
1085	ν_{as} PO_3^{2-} in Q^1. PO_2 in Q^2	[38]
1154	ν_s PO_2^- in Q^2	[34–36]
1260	ν_{as} PO_2^- in Q^2	[34–36]
Raman		
695	P-O-P in chains	[38–40]
1020	ν_sNBO in Q^1	[38–40]
1090	Terminal oxygen bond	[38–40]
1175	ν_s PO_2 chains	[38–40]
1250	ν_{as} PO_2 chains	[38–40]
1320	P=O	[38–40]

Young's modulus, its variation, as a function of the glass composition, can be estimated with a good approximation from the following relation:

$$E = 2 \sum_i x_i G_i \sum_i x_i C_i$$

where G_i and C_i are the dissociation energy per unit volume and the compacity factor of the oxyde i with the molar content x_i, respectively. Details for the calculation of these physical quantities are given in [31]. Using thermodynamic data from [32], the calculation gives almost 56 GPa for both the parent glass and the one with the highest silver oxide content. As a consequence, a small amount of Ag_2O doesn't modify the mechanical properties of the parent glass.

All the absorption bands in the FTIR-ATR spectra (Fig. 3a) can be attributed to the phosphate glass network. The main band at ~880 cm^{-1} is attributed to P-O-P asymmetric stretching of bridging oxygen in Q^2 units (ν_{as} P-O-P Q^2) [33–35]. The shoulder centered at ~980 cm^{-1} and the band peaking at 1085 cm^{-1} correspond to the symmetric and asymmetric stretching vibration of PO_3^{2-} in Q^1 units, respectively [34–36]. The band at 1085 cm^{-1} can be attributed to an overlap between PO_3 Q^1 terminal group and PO_2 Q^2 groups in metaphosphate [37]. The shoulder at 1154 cm^{-1} and the absorption band at 1260 cm^{-1} correspond to symmetric and asymmetric vibration of PO_2^- in Q^2 units, respectively [34–36]. The absorption 3 band located at 718 and 775 cm^{-1} are characteristic of P-O-P symmetric stretching vibration in metaphosphate structure [38]. Only little change could be seen in the FTIR-ATR spectra when Ag_2O increases. The decrease in the absorption band located at 1260 cm^{-1} indicates a decrease in the network connectivity and an increasing amount of Q^1 units. This is further confirmed from the analysis of the Raman spectra of the glasses (Fig. 3b). The band at around 695 cm^{-1} corresponds to symmetric vibration P-O-P in metaphosphate type chains, the band at 1020 cm^{-1} to symmetric stretch mode of NBO in Q^1 units, and the ones at 1175 cm^{-1} and 1250 cm^{-1} to, respectively, symmetric and antisymmetric vibrations of PO_2 also in phosphate chains [38–40]. The shoulder at ~1090 cm^{-1} corresponds to motion of terminal oxygen bond vibration in phosphate chains [41]. The shift of all the bands toward lower wavenumber indicates a weakening of the chemical bonds in the network when Ag_2O is added in the network, due to a network depolymerization. The increase in intensity of the bands at 695 and 1020 cm^{-1} along with the increase in intensity of the shoulder at 1090 cm^{-1} further confirm the increase in Q^1 units and the shortening of the phosphate chain. This change in the glass structure induced by an increase in Ag_2O is in agreement with the shift of the optical band gap toward higher wavelength when Ag_2O increase (Fig. 8). The increase in the intensity of the shoulder at 1090 cm^{-1} along with the shift of the optical band gap indicates an increasing number of non-bridging terminal oxygens [42]. This is expected as the overall phosphate content decreases at the expense of the glass modifier elements [43]. Furthermore the small shoulder at 1320 cm^{-1} related to P=O remains unchanged indicating that the amount of Q^3 is similar in all investigated samples. A summary of the band attribution can be found in Table 3.

Typically an increase in Q^1 units leads to an increase in the glass chemical durability [7, 44]. However, in the studied glasses this seems not to be the case. As shown in Fig. 4, it is clear that the decrease in the solution pH is steeper with an increase in the Ag content. Furthermore, the ICP-OES results show that with increasing the immersion time, the Ca, Na, Sr and P are being released in solution. The increased dissolution rate with increasing Ag content is clearly seen from the higher content of each element in the solution. Except for Na, all the curves present a parabolic shape. It seems that the element release follows a $t^{1/2}$ law which is typical for a diffusion controlled process. However, the parabolic shape of the ion release could also come from the saturation of the solution with those ions leading to the precipitation of a reactive layer. The final Na concentration appears to be high, compared to the amount of the other ions, if a congruent dissolution is assumed [7]. Typically Na is the first element to leach out in solution upon dissolution of phosphate glasses. Furthermore, no Na is usually found in the reactive layer precipi-

Table 4: $(M^{I,II}/P)_{layer}$ / $(M^{I,II}/P)_{core}$ values with the corresponding standard deviations.

	Na/P	Ca/P	Sr/P
Parent glass	1.00	1.00	1.00
x=2-2w	0.24	1.59	1.46
	(0.03)	(0.07)	(0.10)
x=5-2w	0.32	1.31	1.25
	(0.03)	(0.09)	(0.09)

tating at the surface of bioactive glasses [11]. The Ag content was not quantified by ICP as the noise to signal ratio was too high to draw any clear conclusion.

The FTIR-ATR spectrum of the glasses was recorded at each immersion time point. From Fig. 6a, it is clear that at 168 h of immersion, structural modification occurs at the surface of the glasses. All glasses present a disruption of the Q^2 units with a subsequent increase of the Q^1 units. This is attributed to the first phase of phosphate bioactive glass reaction in physiological medium [7, 11]. The shift to lower wavenumber of the bands attributed to Q^2 units also confirms a weakening of the bonds strength for these structural units. The phosphate chains breakage is found to proceed up to the longest immersion time. In a first time, as explained by Bunker *et al.*, it appears that the glass dissolution is controlled by the rate at which the water diffuses at the surface of the glass. Once a full phosphate chain is surrounded by OH group it is released in solution [7]. This explains that ICP results reveal a perfect match between the ions released in solution and the ion concentration of the parent glass (congruent dissolution). At longer immersion time P-O-P bond breakage occurs as seen by the change in Q^2 to Q^1 ratio in the FTIR-ATR spectra. However, while the glass with x=0 only show the disruption of the phosphate chains at the surface of the particles (Fig. 6a), the spectra of all Ag-containing glasses (Fig. 6b–6d) present a sharp increase in Q^1 units and appearance of new bands at 988 and 1030 cm^{-1}, after 673 h of immersion. The new bands have been attributed to the formation of a CaP layer at the surface of the glass particles [11]. As shown in Fig. 6e, with an increase in Ag_2O the signal related to the CaP layer becomes stronger, as evidenced by the increasing intensity of the peaks at 988 and 1030 cm^{-1}. This might be attributed to the faster dissolution rate with increasing Ag_2O, which leads to faster saturation of the solution toward the reactive layer formation. The layer forming at the surface was analyzed via EDS/SEM. While the layer could be sparsely seen at the surface of the undoped glass (x = 0) even after the longest immersion time, the glasses with x = 3 and 5 mol% showed clear sign of CaP precipitation (as shown by the arrow in Fig.7b and 7c) already happening after 332 h of immersion. As the dissolution rate increases with Ag_2O, the layer thickness of the reactive layer was found to be thicker for the glass with higher Ag content. The EDS analysis confirmed that the layer was enriched in Ca and Sr, while Na was preferentially released in the solution. This is illustrated by the different ratios between the $M^{I,II}/P$ values obtained for the layer divided by those obtained for the core of the glass particles. These ratios are summarized in Table 4.

Furthermore, when comparing the EDS composition of all reactive layers, at the surface of all investigated glasses, a typical layer composition could be expressed as follow: 59±3%P, 24±4%Ca, 15±3%Sr, 1±1%Na, 0±1%Ag. Even more the layer was found of be free of Na and Ag. In addition, the average value of the (Ca+Sr)/P ratio for the layer is 0.7±0.1 and is higher than those of the parent glass (0.4). Based on this ratio, as well as the position of the new absorption bands appearing in the FTIR-ATR spectra one can assume that the layer forming is a Sr-substituted calcium-phosphate chemically close to the dibasic calcium phosphate, as seen previously [11]. Moreover, the layer composition was found to be independent of the Ag concentration. This can further explain the higher final level of Na in solution compared to the other ions. Ag appears to behave similarly as Na, *i.e.* it is not incorporated in the reactive layer and thus Ag is expected to leach out at a similar rate than Na. Such layer was found to promote the adhesion and proliferation of human gingival fibroblasts [12]. Furthermore, the controlled release of Ag as monovalent ions may be of interest for its antimicrobial properties.

5 Conclusion

The addition of Ag_2O in a phosphate bioactive glass, with composition $0.5P_2O_5{\cdot}0.2CaO{\cdot}0.2SrO{\cdot}0.1Na_2O$, leads to a glass with shorter phosphate chains and higher number of terminal non bridging oxygen, as evidenced by the increase in Q^1 units and the shift of the optical band gap towards higher wavelength. Adding up to 3 mol% of Ag_2O was also found to increase the processing window. Despite the decrease in the chain length, the decrease in network connectivity as evidenced by a progressive decrease in T_g when Ag_2O increases, leads to a glass more prone to react in aqueous solution. The formation of a Sr-substituted calcium phosphate layer was found to occur sooner in the Ag-containing glass due to the increased dissolution rate. However the layer composition was found to be indepen-

dent of the Ag content. Finally the Ag-containing glasses were found to dissolve in a congruent manner. Such materials could be employed for processing of implants with high surface area to volume ratio, with subsequent antimicrobial properties.

Acknowledgement: The authors would like to acknowledge the Academy of Finland for the financial support of JM through the Academy Research Fellow and Initial Research Cost.

References

[1] L.L. Hench, R.J. Splinter, W.C. Allen, T.K. Greenlee, J Biomed Mater Res Symp, 334 (1971), 117–141
[2] O.H. Andersson, K. H. Karlsson, K. Kangasniemi, A. Yli-Urpo, Glastechnische Berichte 61(10) (1988), 300–305
[3] S. Fagerlund, J. Massera, M. Hupa, L. Hupa, J Eur Ceram Soc 32 11(8) (2012), 2731–2738
[4] E. Pirhonen E, H. Niiranen, T. Niemelä, M. Brink P. Törmälä, J Biomed Mater Res B Appl Biomater 77(2) (2006), 227–33
[5] D. Groh, F. Döhler, D.S. Brauer, Acta Biomat., 10(10) (2014), 4465–4473
[6] J. Massera, S. Fagerlund, L. Hupa, M. Hupa, Journal of the American Ceramic Society, 95 (2012), 607–613
[7] B.C. Bunker, G.W. Arnold, J.A. Wilder, J. Non Crys Solids 64 (3) (1984), 291–316
[8] J. Clement, J.M. Manero, J.A. Planell, J Mater Sci: Mater Med 10 (1999), 729-32.
[9] I. Ahmed, M. Lewis, I. Olsen, J.C. Knowles, Biomaterials 25 (2004), 501–507
[10] J. Massera, Y. Shpotyuk, F. Sabatier, T. Jouan, C. B. Plédel, C. Roiland, B. Bureau, L. Petit, N.G. Boetti, D. Milanese, L. Hupa, J Non Crys Sol 425 (2015), 52–60
[11] J. Massera, L. Petit, T. Cardinal, J. J. Videau, M. Hupa, L. Hupa, J Mater Sci: Mater Med (24) (2013), 1407–1416
[12] J. Massera, A. Kokkari, T. Narhi, L. Hupa, J Mater Sci: Mater Med 26 (2015), 196
[13] V. Salih, K. Franks, M. James, W. Hastings, C. Knowles, I. Olsen, J Mater Sci: Mater Med 11 (2010) 615-620
[14] I Ahmed, D. Ready, M. Wilson, J.C. Knowles, Journal of Biomedical Research Part A, 79 (2006) 618–626
[15] C. Wu, Y. Zhou, M. Xu, P. Han, L. Chen, J. Chang, Y. Xiao, Biomaterials, 34 (2013) 422–433
[16] G. Poongodi, P. Anandan, R.M. Kumar, R. Jayavel, Spectrochimica Acta Part A: molecular and Biomolecular Spectroscopy, 148 (2015) 237–243.
[17] A.P. Adams, E.M. Santschi, M.A. Mellencamp, Vet. Surg. 28 (1999), 219–225
[18] H.S. Carr, T. Wlodkowski, H.S. Rosankranz: Silver sulfadiazine Che-mother 4 (1973), 585–587
[19] S. P. Valappil, D. M. Pickup, D. L. Carroll, C. K. Hope, J. Pratten, R. J. Newport, M. E. Smith, M. Wilson, J. C. Knowles, Antimicr Ag and Chemo 51 (12) (2007), 4453–4461.
[20] I. Ahmed, E.A. Abou-Neel, S.P. Valappil, S.N. Nazhat, D.M. Pickup, D. Carta, D.L. Caroll, R.J. Newport, M.E. Smith, J.C. Knowles, Journal of Materials Science, 42 (2007) 9827–9835
[21] A.A. Ahmed, A.A. Ali, Doaa A.R. Mahmoud, A.M. El-Fiqi, Solid State Sciences, 13 (2011) 981–992
[22] G. V. Blessing, ASTM STP 1045, Philadelphia, PA, USA (1990) 1045
[23] S. Chenu, J. Rocherullé, R. Lebullenger, O. Merdrignac, F. Cheviré, F. Tessier, H. Oudadesse, Journal of Non-Crystalline Solids 356 (2010) 87–92
[24] S. Chenu, R. Lebullenger, J. Rocherullé, Journal of Material Science, 45 (2010) 6505–6510
[25] C. Petitjean, P.J. Panteix, C. Rapin, M. Vilasi, R. Podor, Procedia Materials Science, 7 (2014) 101–110
[26] J.A. Duffy, J Non-Cry Sol 196 (1996), 145-50
[27] T. N. Kim, Q.L. Feng, J.O. Kim, J. Wu, H. Wang, G.C. Chen, F.Z. Cui, J Mater Sci Mater Med. 9(3): (1998) 129–134
[28] S.D. Stookey, Ind. Eng. Chem, 51 (1959), 805–808
[29] A.S. Kuznetsov, Ngo T. Cuong, V.K. Tikhomirov, M. Jivanescu, A. Stesmans, L.F. Chibotaru, J.J. Velázquez, V.D. Rodríguez, D. Kirilenko, G. Van Tendeloo, V.V. Moshchalkov, Opt Mat, 34 (2012), 616–621
[30] J. Massera, A. Martin, J. Choi, T. Anderson, L. Petit, M. Richardson, Y. Obeng, K. Richardson, J Phy Chem Sol, 71 (2010), 1634–1638
[31] J. Rocherullé, C. Ecolivet, M.Poulain, P. Verdier, Y. Laurent, J. of Non-Cryst. Solids 108 (1989) 187–193
[32] D.D. Wagman, W.H. Evans, V.B. Parker, I. Halow, R.H. Schumm, Selected values of chemical thermodynamic properties, NBS technical notes, 270, 3–9, 1981
[33] P.Y. Shih, H.M. Shiu, Mater Chem Phy 106: (2007), 222–226.
[34] H. GaO, T. Tan, D. Wang, J of Contr Rel 96: (2004), 21–28.
[35] Y.M. Moustafa, K. El-Egili, J Non-Crys Sol, 240: (1998), 144–153
[36] E.A. Abou Neel, W. Chrzanowski, D.M. Pickup, L.A. O'Deel, N.J. Mordan, R.J. Newport, M.E. Smith, J.C. Knowles, J Roy Soc Inter, 6: (2009), 435–446.
[37] D. Ilieva, B. Jivov, G. Bogachev, C. Petkov, I. Penkov, Y. Dimitriev, J Non-Crys Sol, 283 (2001), 195–202.
[38] S. Lee, A. Obata, T. Kasuga, J Cer Soc Jap, 117 (2009), 935–938
[39] M.A. Karakassides, A. Saranti, I. Koutselas, J Non-Crys Sol 347 (2004), 69–79.
[40] A.G. Kalampounias, J Phy Chem Sol, 73 (2012), 148–153.
[41] R. C. Lucacel, A.O. Hulpus, V. Simon, I. Ardelean, J Non-Crys Sol,355: (2009), 425–429.
[42] J. Massera, M. Vassallo-Breillot, B. Törngren, B. Glorieux, L. Hupa, J Non-Crys Sol, 402 (2014), 28–35
[43] R.K. Brow, Journal of Non Crystalline Solids, 263–264 (2000), 1–28
[44] J. Massera, K. Bourhis, L. Petit, T. Cardinal, L. Hupa, M. Hupa, Journal of Physics and Chemistry of Solids, 74 (2013) 121–127.